

21 **ABSTRACT**

22 This study presents an analytical framework to estimate the change in ultimate bearing capacity of
23 energy piles in unsaturated fine-grained soils under drained mechanical loading conditions after
24 drained heating. The framework was developed by extending conventional methods for the
25 ultimate bearing capacity of piles in unsaturated soils to temperature-dependent conditions, where
26 thermally induced changes in the characteristics of the unsaturated soil and soil-pile interface are
27 considered. Specifically, the thermally induced variations in matric suction and effective saturation
28 profiles with depth were incorporated into calculations of the shaft capacity and the end bearing
29 capacity of piles in unsaturated soils. The proposed ultimate bearing capacity model is validated
30 against experimental data for an energy pile loaded to failure in unsaturated Bonny silt, and a good
31 match between measured and predicted values was obtained. A parametric study was carried out
32 to evaluate the effects of flow rate and aspect ratio (i.e., pile embedment length/pile diameter) on
33 the ultimate bearing capacity of energy piles in unsaturated clay and silt subject to temperatures
34 ranging from 5 to 45 °C. For both soils, the shaft, end bearing, and ultimate bearing capacities vary
35 with an increase in temperature. At reference temperature, the shaft, end, and ultimate bearing
36 capacities monotonically vary with pile embedment length whereas, at elevated temperatures, they
37 vary non-monotonically with pile embedment depth. At given temperature, the parametric study
38 shows that the bearing capacity of energy piles in clay decreases and in silt decreases or increases
39 depending on pile embedment length with increasing downward infiltration of water into the soil
40 profile surrounding the energy pile. The ultimate bearing capacity increases with a decrease in the
41 aspect ratio at all temperatures. Estimates of the ultimate bearing capacity of energy piles in
42 unsaturated fine-grained soils from the framework are a critical part of thermo-mechanical soil-
43 structure interaction analyses needed to design energy piles, so this study contributes toward the
44 widespread application of this emerging technology in practice.

45 **KEYWORDS**

46 Unsaturated soils; Energy piles; Bearing capacity; Temperature; Fine-grained soils

47 INTRODUCTION

48 Deep foundations are extensively used in various geotechnical and geoenvironmental applications
49 to transfer mechanical loads to firm strata, resist horizontal and uplift movements, and minimize
50 settlements. Estimating the ultimate bearing capacity of a deep foundation is an important step in
51 their geo-structural design. Most methods used in practice for estimating the ultimate bearing
52 capacity of deep foundations are focused on saturated soils (e.g., Skempton 1959; Chandler 1968;
53 Burland 1973), and only in the past two decades have studies focused on the behavior of deep
54 foundations in unsaturated soil layers. For instance, Georgiadis et al. (2003) used finite element
55 analysis to study the influence of unsaturated soil conditions on the behavior of piles while
56 Vanapalli and Taylan (2012) extended methods originally developed for saturated soils to
57 unsaturated soils under both drained and undrained mechanical loading.

58 Over the past decade, there has been a rapidly growing interest toward integrating
59 geothermal heat exchangers into deep foundations to improve the efficiency of heating and cooling
60 systems for buildings (e.g., Brandl 2006; Laloui et al. 2006; Loveridge et al. 2019; McCartney et
61 al. 2019; Laloui and Rotta Loria 2019). During heat exchange operations, the temperature of these
62 piles (referred to as energy piles) typically varies between 5 and 35 °C (e.g., McCartney and
63 Murphy 2017), although some laboratory studies have evaluated the effects of temperatures as
64 high as 45 °C (Xiao et al. 2014; Liu et al. 2019; Goode and McCartney 2015). In energy piles,
65 axial stresses may be induced by heating that are superimposed atop the axial stresses due to
66 mechanical loading. Although it is desirable for the combined thermo-mechanical stresses to be
67 within the elastic range, the temperature changes can affect the soil surrounding the pile and, in
68 turn, affect the ultimate bearing capacity. The majority of previous studies on the ultimate bearing
69 capacity of energy piles are limited to dry or saturated conditions (Kramer and Basu 2014; Wang

70 et al. 2014; Ng et al. 2015; Gunawan et al. 2015; Goode and McCartney 2015) and fewer studies
71 have focused on unsaturated conditions (Uchaipichat 2005, 2012, 2013; McCartney and Rosenberg
72 2011; Goode and McCartney 2015; Akrouch et al. 2016). Knowledge of the ultimate bearing
73 capacity of energy piles is critical in thermo-mechanical load transfer (T-z) analyses, so
74 understanding the impact of unsaturated conditions on the components of the ultimate bearing
75 capacity will lead to improved designs considering soil-structure interaction (e.g., Knellwolf et al.
76 2011; Chen and McCartney 2016). Gaps remain for an analytical framework that can reasonably
77 capture the effects of temperature on the ultimate bearing capacity of energy piles in unsaturated
78 soils.

79 This study aims to provide insight into the effects of temperature and unsaturated
80 conditions on the ultimate bearing capacity of energy piles with a practical goal of facilitating the
81 computationally efficient design and analysis of energy piles in unsaturated soils. For this purpose,
82 this paper presents an analytical framework built on fundamental theories to estimate the ultimate
83 bearing capacity of energy piles in unsaturated soils subject to varying temperatures under drained
84 heating and mechanical loading conditions. A temperature-dependent model for effective stress is
85 incorporated into the formulation of the shaft and end bearing capacity of the energy pile. The
86 proposed model includes the effect of temperature on matric suction, degree of saturation, and
87 pile-soil interface strength. The model is validated against data available in the literature. A
88 parametric study is carried out to evaluate the effects of flow rate and aspect ratio (i.e., pile
89 embedment length/pile diameter) on the ultimate bearing capacity of an energy pile in clay and silt
90 at temperatures ranging from 5 to 45 °C.

91 **BACKGROUND**

92 The ultimate bearing capacity of an energy pile is expected to vary during drained heating due to
93 the effects of temperature on the properties of the soil, pile, and soil-pile interface. Results of tests
94 in the literature report different trends of ultimate bearing capacity of energy piles with
95 temperature. McCartney and Rosenberg (2011) observed a 40% increase in the ultimate capacity
96 of an energy pile in unsaturated Bonny silt after heating the pile in the centrifuge by 41 °C.
97 However, they did not characterize the changes in water content of the soil surrounding the energy
98 pile during heating. Wang et al. (2014) tested a pile in silt at 1g and found that the ultimate capacity
99 of pile at 38 °C was higher than that at 20 °C. Ng et al. (2015) performed centrifuge tests on energy
100 piles in saturated sand and found that an increase in ultimate bearing capacity of 13% occurred
101 primarily due to changes in shaft capacity when the pile was heated from 22 to 37 °C. However,
102 they observed a larger increase in ultimate bearing capacity of 30% occurred primarily due to
103 changes in end bearing capacity when the pile was heated from 22 to 52 °C. Many investigators
104 have developed semi-analytical or numerical models to study the effect of temperature on soil-
105 structure interaction, although most did not consider the effect of temperature on the bearing
106 capacity (e.g., Knellwolf et al. 2011; Suryatriyastuti et al. 2013, 2014; Olgun et al. 2014; Saggi
107 and Chakraborty 2015; Chen and McCartney 2017). Further, other studies have compared results
108 from numerical simulations with thermal stress and strain data from heating tests on full-scale
109 energy piles (e.g., Di Donna and Laloui 2013; Di Donna et al. 2016a; Rotta Loria et al. 2015;
110 Fuentes et al. 2016; Fu 2017). Several of these studies have found that an increase in temperature
111 leads to increases in the magnitude of the shaft and end bearing capacities of the pile.

112 The effect of temperature on the properties of the soil-energy pile interface is another factor
113 that can influence the ultimate bearing capacity of energy piles. Akrouch et al. (2014) and Yavari

114 et al. (2016) reported negligible changes in the interface friction angle and adhesion of soil-pile
115 interfaces. Murphy and McCartney (2014) performed borehole shear tests with heated concrete
116 interface pads and found negligible changes in interface friction angle with temperature. Di Donna
117 et al. (2016b) conducted tests on saturated clay-concrete interfaces at different temperatures and
118 found an increase in the apparent adhesion and a reduction in interface friction angle during
119 heating. Fu (2017) observed that an increase in temperature can cause a decrease in water content
120 and an increase in the interface friction angle and adhesion for interfaces between concrete and
121 unsaturated soil. Yazdani et al. (2018) performed a set of laboratory tests and found that the shear
122 strength of a saturated clay-concrete pile interface increases with temperatures from 24 to 34 °C,
123 possibly due to changes in clay volume at the interface. Vasilescu et al. (2019) observed only small
124 changes in the interface friction angle (i.e., within 0.7 degrees) for a saturated soil-concrete pile
125 interface sheared at temperatures of 8, 13, and 18 °C.

126 There are only very few studies that have investigated energy piles under unsaturated
127 conditions. However, existing studies show the overall performance of energy piles is affected by
128 the unsaturated conditions and temperatures (e.g., McCartney and Rosenberg 2011; Goode and
129 McCartney 2015; Wang et al. 2012; Uchaipichat 2013; Akrouch et al. 2014; Fu 2017; Behbehani
130 and McCartney 2020a, 2020b; Thota and Vahedifard 2020). Wang et al. (2012) reported a
131 reduction in the shaft capacity of a pile in fine sand with initial gravimetric water contents of 0, 2,
132 and 4% when the pile temperature was increased from 20 to 60 °C, although they studied an
133 aluminum energy pile that may have mobilized a fraction of the ultimate capacity during heating
134 prior to mechanical loading. Goode and McCartney (2015) performed centrifuge tests on a model
135 thermo-active pile embedded in silt. They observed a decrease in water content and an increase in
136 pile shaft capacity because of heating the pile from room temperature to 41 °C. Behbehani and

137 McCartney (2020a) used a coupled thermo-hydro-mechanical model to explain that this increase
138 in capacity was due to thermally induced drying of the surrounding soil during monotonic heating,
139 which led to an increase in effective stress and shear strength. Behbehani and McCartney (2020b)
140 used this model to study the seasonal cyclic heating and cooling response of energy piles and found
141 only minor changes in degree of saturation with time, indicating that drained conditions can be
142 assumed. Coupled heat transfer and water flow models may provide the best interpretation of the
143 transient processes in unsaturated soils surrounding energy piles, but simplified analytical
144 approaches are preferred for energy pile design.

145 **MODEL DEVELOPMENT**

146 **Conceptual Model of Ultimate Bearing Capacity of Piles under Varying Temperatures**

147 Proper design of energy piles warrants a careful examination of all parameters that are affected by
148 changes in hydraulic and mechanical loads under varying temperatures. In this study, the ultimate
149 bearing capacity of an energy pile in an unsaturated soil layer is determined by quantifying the
150 shaft and end bearing capacities under varying degrees of saturation and temperatures. The effects
151 of degree of saturation (or suction) and temperature are accounted for in the properties of the
152 surrounding unsaturated soil, and as well as the soil-pile interface under drained mechanical
153 loading conditions. The temperature distribution within the pile is assumed to be constant and
154 heating is assumed to be drained (i.e., all thermal volume changes in the soil have occurred and
155 there are no excess pore water pressures or changes in degree of saturation). These assumptions
156 can reasonably represent field conditions in which the changes in the average temperature of the
157 energy pile occur slowly over several months and sufficient time is permitted for dissipation of
158 pore water pressures (Behbehani and McCartney 2020b). For these conditions, it can also be
159 assumed that the soil surrounding the energy pile reaches an almost constant temperature along

160 the pile length. Several studies including field and laboratory tests observed constant soil
161 temperatures along the length of the pile (e.g., Laloui et al. 2006; Bourne-Webb et al. 2009;
162 Kalantidou et al. 2012; Murphy et al. 2015; Ng et al. 2015; McCartney and Murphy 2017;
163 Vasilescu et al. 2019; Elzeiny et al. 2020). Increases in pile dimensions due to thermal expansion
164 are not considered. Several studies (e.g. Knellwolf et al. 2011; Chen and McCartney 2017) have
165 shown that thermally induced changes in the pile dimensions are small enough that they do not
166 result in significant changes in radial stress and side shear restraint. Further, the change in length
167 of the energy pile is not significant enough to change the area used in the calculation of the shaft
168 capacity.

169 The temperature in the pile induces thermal changes in the matric suction and degree of
170 saturation in the soil, which will affect the effective stress and apparent cohesion in the soil, which
171 will affect the ultimate bearing capacity. The magnitude of thermally induced variation in the
172 ultimate bearing capacity of an energy pile depends on the soil type and pile embedment depth.
173 Triggered by changes in hydraulic properties and apparent cohesion, thermal induced changes in
174 the pile-soil interface strength can also affect the ultimate bearing capacity. At the edge of the pile,
175 the thermally induced water flow in unsaturated soils occurs due to several phenomena arising
176 from temperature effects on water properties (density, viscosity, surface tension, etc.), soil-water
177 retention properties, and vapor diffusion (Philip and De Vries 1957; Grant 2003; Başer et al. 2018;
178 Behbehani and McCartney 2020a, 2020b). These factors together cause water to flow through the
179 soil away from the pile, leading to desaturation which in turn can affect the thermal efficiency of
180 the energy pile (e.g., Akrouch et al. 2016). This is mainly due to the lower thermal conductivity of
181 dry and unsaturated soils compared to saturated soils (Campbell et al. 1994; Lu and Dong 2015).
182 This study attempts to develop a framework to investigate the effect of changes in hydraulic

183 profiles with drained heating and their impact on the ultimate bearing capacity of piles under
184 drained mechanical loading. This is achieved by considering the effect of temperature on suction
185 profile through a combination of water retention mechanisms and water properties with Darcy's
186 law. For simplicity and to avoid complex coupled mass and energy analyses, this study ignores the
187 effect of thermally induced vapor diffusion and phase change on the ultimate bearing capacity of
188 energy piles. Heat transfer was also not considered in the model, and it was assumed that the pile
189 and soil at the pile-soil interface were at equilibrium under an applied value.

190 **Drained Heating**

191 The shear strength and bearing capacity of unsaturated soils are mainly controlled by changes in
192 matric suction and degree of saturation. Thus, the first step towards developing the temperature-
193 dependent formulation for the ultimate bearing capacity involves the determination of matric
194 suction and degree of saturation profiles under drained heating conditions.

195 Building upon the effective stress principle of Bishop (1959), the suction stress-based
196 effective stress of unsaturated soils was defined by Lu et al. (2010) as:

$$197 \quad \sigma' = (\sigma - u_a - \sigma^s) \quad (1)$$

198 where σ is the total stress, u_a is the pore-air pressure, and σ^s is the suction stress, which can be
199 represented as (Lu et al. 2010):

$$200 \quad \sigma^s = -\psi S_e \quad (2)$$

201 where ψ is the matric suction and S_e is the effective degree of saturation. The suction stress can
202 be used to estimate the shear strength of unsaturated soils using the Mohr-Coulomb failure criteria,
203 as follows (Lu et al. 2010; Vahedifard et al. 2016):

204
$$\tau = c' + (\sigma - u_a - \sigma^s) \tan \phi' \quad (3)$$

205 where τ is the shear strength, c' is the effective cohesion arising from cementation, ϕ' is the
 206 effective friction angle. The above formulations (Eqs. 1 to 3), which were originally defined under
 207 ambient temperature conditions, can be extended to temperature-dependent conditions by
 208 incorporating temperature-dependent matric suction and the soil water retention curve (SWRC)
 209 (Vahedifard et al. 2018, 2019). The impact of temperature on the matric suction can be expressed
 210 as follows (Grant and Salehzadeh 1996):

211
$$\psi = \psi_{T_r} \left(\frac{\beta + T}{\beta_{T_r} + T_r} \right) \quad (4)$$

212 where ψ_{T_r} is the matric suction at the reference temperature T_r . As defined, β_{T_r} is a regression
 213 parameter at the reference temperature, which depends on surface tension, enthalpy of immersion
 214 per unit area, and contact angle. The parameter β is calculated as (Grant and Salehzadeh 1996):

215
$$\beta = \frac{-\Delta h T_r}{-\Delta h + a (\cos \alpha')_{T_r} + b (\cos \alpha')_{T_r} T_r} \quad (5)$$

216 where α' is the temperature-dependent soil-water contact angle, a and b are fitting parameters that
 217 can be estimated as $a = 0.11766 \text{ Nm}^{-1}$ and $b = -0.0001535 \text{ Nm}^{-1}\text{K}^{-1}$ (Dorsey 1940; Haar et al.
 218 1984) and Δh is the enthalpy of immersion per unit area, which can be determined by
 219 experimental measurements or by using the differential enthalpy of adsorption of the vapor
 220 (Vahedifard et al. 2020). Grant and Salehzadeh (1996) neglected the effect of temperature on the
 221 enthalpy of immersion even though Watson (1943) demonstrated that temperature could affect the
 222 enthalpy of immersion as well. In this study, as suggested by Vahedifard et al. (2018, 2019), the

223 following temperature-dependent equation of Watson (1943) is used to define the enthalpy of
 224 immersion per unit area:

$$225 \quad \Delta h = \Delta h_{T_r} \left(\frac{1-T_r}{1-T} \right)^{0.38} \quad (6)$$

226 where Δh_{T_r} is the enthalpy of immersion per unit area at the reference temperature.
 227

228 The temperature-dependent form of the soil-water contact angle is given as (Grant and
 229 Salehzadeh 1996):

$$230 \quad \cos \alpha = \frac{-\Delta h + TC_1}{a' + bT} \quad (7)$$

231 where C_1 is a constant, which can be determined as (Grant and Salehzadeh 1996):
 232

$$233 \quad C_1 = \frac{\Delta h_{T_r} + a(\cos \alpha)_{T_r} + b(\cos \alpha)_{T_r} T_r}{T_r} \quad (8)$$

234 The regression parameters and the above equations are thoroughly discussed and validated
 235 in Vahedifard et al. (2018, 2019).

236 Using the Brooks and Corey (1964) SWRC model and the temperature-dependent matric
 237 suction, the temperature-dependent effective saturation can be written as (Vahedifard et al. 2018,
 238 2019):

$$239 \quad S_e = \left(\frac{\psi_{aev}}{\psi \left(\frac{\beta_{T_r} + T_r}{\beta + T} \right)} \right)^{n_{BC}} \quad (9)$$

240 where ψ_{aev} and n_{BC} are fitting parameters representing the air entry parameter and pore size
 241 distribution parameter of the SWRC, respectively.

242 The temperature-dependent equations for matric suction (Eq. 4) and effective saturation
 243 (Eq. 9) can be used along with a simplified flow analysis to estimate the depth profiles of matric
 244 suction and degree of saturation for different water table depths and flow rates. For one-
 245 dimensional vertical liquid water flow in isotropic and homogenous materials, Darcy's law is given
 246 as follows:

$$247 \quad q = -k \left(\frac{1}{\gamma_w} \frac{d\psi}{dz} + 1 \right) \quad (10)$$

248 where k is the hydraulic conductivity, z is the distance above the water table, γ_w is the unit weight
 249 of water, q is the steady vertical fluid flow rate (zero for hydrostatic, negative for infiltration, and
 250 positive for evaporation). Lu and Griffiths (2004) developed an analytical solution for matric
 251 suction profiles as a function of seepage condition and hydraulic parameters:

$$252 \quad \psi = \frac{\gamma_w}{\beta'} \ln \left[\left(1 + \frac{q}{k_s} \right) e^{-\beta' z} - \frac{q}{k_s} \right] \quad (11)$$

253 where k_s is the hydraulic conductivity of saturated soil. The temperature can affect matric suction
 254 in the soil mass through the interface of air and water phases and porous fluid structure. The
 255 formulation for temperature-dependent matric suction was established and validated by Grant and
 256 Salehzadeh (1996) and Vahedifard et al. (2018, 2019). Thota et al. (2019) defined the one-
 257 dimensional suction profiles in unsaturated soil layers for different temperatures and infiltration
 258 rates, as follows:

$$259 \quad \psi = \frac{\gamma_w}{\psi_{aev}} \ln \left[\left(1 + \frac{q}{k_s} \right) e^{-\psi_{aev} z} - \frac{q}{k_s} \right] \left(\frac{\beta_{T_r} + T_r}{\beta + T} \right) \quad (12)$$

260 The hydraulic conductivity of saturated soil can be affected by temperature because of the
 261 effect of temperature on water viscosity (Pillsbury 1950; Philip 1969). The relationship between
 262 the hydraulic conductivity of saturated soil and temperature is given by (Constantz 1982):

$$263 \quad k_s = \frac{k_{in} \gamma_w}{\eta(T)} \quad (13)$$

264 where k_{in} is the intrinsic permeability assumed to be dependent only on the soil and $\eta(T)$ is the
 265 water viscosity. The water viscosity varies with temperature as follows (Lide 1995):

$$266 \quad \eta(T) = 0.0002601 + 0.001517 \exp[-0.034688 \times (T - 273)] \quad (14)$$

267 Using the SWRC model of Brooks and Corey (1964) and the hydraulic conductivity of
 268 Gardner (1958), the temperature-dependent effective saturation profile with depth can be written
 269 as (Thota et al. 2019):

$$270 \quad S_e = \left\{ \exp \left[\ln \left(\left(1 + \frac{q}{k_s} \right) e^{-\beta_{ae} z} - \frac{q}{k_s} \right) \left(\frac{\beta_r + T_r}{\beta + T} \right) \right] \right\}^{1/n_{BC}} \quad (15)$$

271 Mechanical Loading

272 The ultimate bearing capacity of energy piles in unsaturated soils is generally assumed to be
 273 comprised of two components, the shaft capacity and the end bearing capacity, and is given by:

$$274 \quad Q_{(unsat)} = Q_{s(unsat)} + Q_{e(unsat)} \quad (16)$$

275 where $Q_{(unsat)}$ is the ultimate bearing capacity of the pile, $Q_{s(unsat)}$ is the shaft capacity, and $Q_{e(unsat)}$
 276 is the end bearing capacity.

277 An energy pile is subjected to varying temperatures combined with mechanical loading
 278 during its operation. In this section, the temperature-dependent hydraulic formulations discussed

279 in the previous section are employed to extend the ultimate bearing capacity formulations at
 280 ambient conditions to temperature-dependent conditions, to estimate the temperature-dependent
 281 ultimate bearing capacity. Under drained mechanical loading, the shaft capacity of a pile with
 282 length (L) and diameter (D) embedded in unsaturated soil under ambient temperature is given by:

$$283 \quad Q_{s(unsat)} = [c'_a + \beta_c (\sigma - u_a + \psi S_e)] \pi DL \quad (17)$$

284 where c'_a is the adhesion component of the interface shear strength for saturated conditions
 285 (typically equal to zero unless the soil is cemented), β_c is the Burland-Bjerrum coefficient that
 286 can account for the installation method, and $(\sigma - u_a)$ is the net normal stress. Unlike previous
 287 models for piles in unsaturated soils (e.g., Vanapalli and Taylan 2012), Eq. 17 uses the effective
 288 saturation instead of the degree of saturation and has fewer parameters.

289 Extending Terzaghi's bearing capacity equation to unsaturated conditions, assuming no
 290 surcharge the end bearing capacity of unsaturated soils under drained mechanical loading
 291 conditions is written as:

$$292 \quad Q_{e(unsat)} = [N_c (\sigma - u_a + \psi S_e)] \frac{\pi D^2}{4} \quad (18)$$

293 The ultimate bearing capacity of piles in unsaturated soils under drained mechanical
 294 loading is given by:

$$295 \quad Q_{(unsat)} = [c'_a + \beta_c (\sigma - u_a + \psi S_e)] \pi DL + [N_c (\sigma - u_a + \psi S_e)] \frac{\pi D^2}{4} \quad (19)$$

296 Eq. (19) can be used to estimate the ultimate bearing capacity of an energy pile in
 297 unsaturated soil at ambient temperature conditions and can consider different cases where the
 298 suction and effective saturation vary with depth. In the end bearing capacity term in Eq. (19), the

299 matric suction and effective saturation values correspond to the tip of the pile. In this study, Eq.
300 (19) was extended to account for the effects of temperature on the degree of saturation and matric
301 suction, which affect the effective stress. In other words, the degree of saturation decreases at the
302 pile-soil interface due to thermally induced water flow away from the interface, the matric suction
303 increases, and the degree of saturation decreases (Goode and McCartney 2015; Fu 2017).
304 Therefore, the changes in the shear strength of the pile-soil interface can be captured by
305 incorporating thermally induced changes in the SWRC, apparent cohesion (stemming from matric
306 suction), and effective stress. The temperature dependency of pile-soil interface strength can be
307 defined as follows:

$$308 \quad \tau_T = (\sigma - u_a) \tan \delta' + c'_a + c_{app,T} \quad (20)$$

$$309 \quad c_{app,T} = -\sigma^s \tan \delta' \quad (21)$$

310 where τ_T is the interface shear strength and $c_{app,T}$ is the apparent cohesion, which can be defined
311 as a function of depth and temperature as follows:

$$312 \quad c_{app,T} = \tan \delta' \left\{ \exp \left[\ln \left(\left(1 + \frac{q}{k_s} \right) e^{-\psi_{aev} z} - \frac{q}{k_s} \right) \left(\frac{\beta_{T_r} + T_r}{\beta + T} \right) \right] \right\}^{1/n_{BC}} \quad (22)$$

$$\frac{\gamma_w}{\psi_{aev}} \ln \left[\left(1 + \frac{q}{k_s} \right) e^{-\psi_{aev} z} - \frac{q}{k_s} \right] \left(\frac{\beta_{T_r} + T_r}{\beta + T} \right)$$

313 Eqs. 20 and 21 were developed based on the assumption that within the temperature range
314 examined, the effect of temperature on the interface shear strength is controlled by thermally
315 induced changes in apparent cohesion and that temperature has a negligible effect on the interface
316 friction angle. The latter is consistent with the trends reported by most experimental test results in
317 which the temperature is shown to have minimal effects on the effective angle of friction at critical
318 state (e.g., Hueckel et al. 1998; Graham et al. 2001; Li et al. 2019).

319 Using the temperature-dependent matric suction and effective degree of saturation profiles
 320 introduced in the above sections, the temperature-dependent model for the ultimate bearing
 321 capacity of an energy pile in unsaturated soils under drained conditions can be written as:

$$\begin{aligned}
 322 \quad Q_{(unsat)} = & \left[c'_{a,T} + \beta_c \left(\sigma - u_a + \frac{\gamma_w}{\psi_{aev}} \ln \left[\left(1 + \frac{q}{k_s} \right) e^{-\psi_{aev} z} - \frac{q}{k_s} \right] \left(\frac{\beta_r + T_r}{\beta + T} \right) \right) \left\{ \exp \left[\ln \left[\left(1 + \frac{q}{k_s} \right) e^{-\psi_{aev} z} - \frac{q}{k_s} \right] \left(\frac{\beta_r + T_r}{\beta + T} \right) \right] \right\}^{1/n_{BC}} \right] \pi DL \\
 & + \left[c'_{a,T} + N_c \left(\sigma - u_a + \frac{\gamma_w}{\psi_{aev}} \ln \left[\left(1 + \frac{q}{k_s} \right) e^{-\psi_{aev} z} - \frac{q}{k_s} \right] \left(\frac{\beta_r + T_r}{\beta + T} \right) \right) \left\{ \exp \left[\ln \left[\left(1 + \frac{q}{k_s} \right) e^{-\psi_{aev} z} - \frac{q}{k_s} \right] \left(\frac{\beta_r + T_r}{\beta + T} \right) \right] \right\}^{1/n_{BC}} \right] \frac{\pi D^2}{4}
 \end{aligned} \quad (23)$$

323 The first term in Eq. 23 represents the pile shaft capacity contribution, and the second term
 324 represents the pile end bearing capacity contribution. Table 1 shows soil specific parameters and
 325 relevant labroatry tests for saturated and unsaturated conditions. The rest of the parameters (σ_v ,
 326 q , N_c , z , γ_w , L , D) are soil independent parameters. Compared to more conventional formulations
 327 (e.g., for fully saturated conditions), the only added parameters are those for the temperature
 328 dependent SWRC. Eq. 23 offers a unified approach to estimate the ultimate bearing capacity of
 329 energy piles under varying temperatures and vertical flow rates in an unsaturated soil layer.

330 MODEL VALIDATION

331 As noted, limited experimental data is available on the ultimate bearing capacity of energy piles
 332 in unsaturated soils under different temperatures. Accordingly, only the data from centrifuge tests
 333 performed by Goode and McCartney (2015) are used to validate the proposed model. Goode and
 334 McCartney (2015) measured the load-settlement curves of a semi-floating energy pile having a
 335 prototype length of 8.2 m and prototype diameter of 1.5 m embedded in a layer of unsaturated
 336 Bonny silt for pile temperatures of 21, 32, and 40 °C. Dielectric sensors were used to measure the
 337 temperature and the volumetric water content of the soil at a depth of 5.5 m below the pile tip and

338 at a radial distance of 0.6 m from the soil-pile interface, and these results were presented in a
339 follow-on study by Behbehani and McCartney (2020a). As the tests of Goode and McCartney
340 (2015) were performed in compacted soil having a uniform initial suction with depth, Eq. 23 was
341 used to evaluate the ultimate bearing capacity under no-flow conditions ($q = 0$) and constant
342 suction and effective saturation with a depth corresponding to the different temperatures.
343 Specifically, the effects of temperature on the suction and effective saturation were estimated using
344 Eqs. 12 and 15, then were incorporated into Eq. 19.

345 To use the proposed model, we first determined the degree of saturation and the
346 corresponding matric suction at different temperatures using the proposed formulations and
347 compared them against the measured data. Table 2 presents the SWRC parameters used in the
348 calculations. The SWRC parameters shown in Table 2 were obtained by fitting the measured data
349 at the reference temperature ($T = 21$ °C). Fig. 1a shows the predicted SWRCs at different
350 temperatures for Bonny silt. Applying a higher temperature causes the SWRC to shift downward.
351 This means by increasing temperature at a given effective saturation, the matric suction will
352 decrease and at a given matric suction, the effective saturation decreases. The predicted
353 temperature-dependent SWRC models were validated against laboratory measured data in
354 Vahedifard et al. (2018, 2019).

355 A good match is observed between the measured and predicted values of the volumetric
356 water content of unsaturated Bonny silt versus the change in temperature at a prototype distance
357 from the pile of 0.6 m as shown in Fig. 2. The increase in temperature at this location caused a
358 decrease in the volumetric water content of unsaturated silt. The good match in Fig. 2 indicates
359 that the temperature-dependent SWRC may be sufficient to estimate the amount of thermally
360 induced drying in the soil at equilibrium, without having to use a complex transient coupled heat

361 transfer and water flow analysis like used by Behbehani and McCartney (2020a). In the next step,
362 the input parameters shown in Table 2 were used to calibrate the ultimate bearing capacity at
363 reference temperature (i.e., 21 °C). The total stress at mid-height of the pile was considered to be
364 75 kPa at prototype scale. The calibration process was performed by optimizing the β_c value
365 leading to the minimum prediction error against the measured ultimate bearing capacity at 21 °C.
366 The calibrated model was then used with no further fitting to predict the ultimate bearing capacities
367 at higher temperatures at the soil-pile interface (32 °C and 40 °C). A good match is observed
368 between the measured and predicted values of the ultimate bearing capacity of the energy pile in
369 unsaturated Bonny silt versus the change in temperature from room temperature. The comparison
370 shows a good agreement between the measured and predicted values. The increase in temperature
371 at the soil-pile interface causes an increase in the ultimate bearing capacity of the energy pile in
372 unsaturated silt. While the results show a very small error, the proposed model can benefit from
373 further validation from instrumented energy piles in unsaturated soils.

374 **PARAMETRIC STUDY**

375 The proposed framework was employed in a parametric study to evaluate the effect of flow rate
376 and aspect ratio on the ultimate bearing capacity of energy piles in unsaturated clay and silt subject
377 to temperatures ranging from 5 to 45 °C. Table 2 and Figure 1 present the input parameters and
378 the SWRCs, respectively, of Denver bentonite and Bonny silt, which were used in the parametric
379 study. In all cases, the water table was assumed to be at the depth of 20 m below the ground surface.
380 Aspect ratio, AR , is defined as the ratio of the pile embedment length, L , to the pile diameter, D .

381 **Effect of Flow Rate**

382 Three flow rates were examined for each soil including: $q = 0$ (hydrostatic), $q = -1.6E-09$ m/s
383 (infiltration), and $q = -3.0 \times 10^{-9}$ m/s (infiltration) for Denver bentonite, and $q = 0$ (hydrostatic), q

384 = -3.2×10^{-8} m/s (infiltration), and -6.0×10^{-8} m/s (infiltration) for Bonny silt. The flow rates were
385 chosen in such a way that q/k_s at the reference temperature varies between two extreme flow rates
386 (i.e., 0.0 and -0.95) for each soil.

387 Fig. 4 shows the effective saturation, matric suction, and effective stress of Denver
388 bentonite (hereafter referred to as clay) along the pile embedment length at different temperatures
389 and flow rates. For a given pile length, the effective saturation decreases (Fig. 4a), and matric
390 suction increases (Fig. 4b) monotonically with an increase in temperature. On the other hand, the
391 changes in effective stress (Fig. 4c) are monotonic at 5 °C and 25 °C and nonmonotonic at 45 °C.
392 The distinct variation of the properties is mainly due to thermally induced drying and liquid flow
393 in the soil along the pile length. At any given length, as the flow rate changes from hydrostatic to
394 infiltration state, the effective saturation increases and matric suction decreases with an increase
395 in temperature. Depending on the length of the pile and the effective saturation, the effective stress
396 increases or decreases with temperature. Approximately up to 12 m depth from the ground surface,
397 the effective stress increases, and from 12 m to the water table, the effective stress decreases at 45
398 °C, and at the other temperatures (5 °C and 25 °C), the effective stress increases at all pile lengths.
399 At depths close to the water table (near saturation), the temperature has minimal effects on
400 effective stress whereas the temperature effect on effective stress increases as the distance from
401 the water table increases. Thermal induced changes in effective stress can be attributed to the
402 impact of temperature on physiochemical mechanisms of the porous medium, changing effective
403 saturation, and matric suction under different flow conditions. At the water table, since the soil is
404 in a saturated state, the flow rate has no effect on effective stress. It is important to note that the
405 soil in this study is assumed to not deform significantly with changes in temperature, which would
406 cause changes in the ultimate bearing capacity of the soil in saturated conditions (at the location

407 of the water table). This assumption is reasonable for heavily-overconsolidated low-plasticity soils,
408 but the effects of volume change of saturated soils on the shaft capacity of energy piles have been
409 observed in the literature (e.g., Ozudogru et al. 2015; Ravera et al. 2020).

410 Fig. 5 shows the variation of shaft capacity, end bearing capacity, and ultimate bearing
411 capacity versus the pile embedment length for clay at temperatures 5, 25, and 45 °C under three
412 flow rates with $AR = 10$. As shown in Fig. 5a, for a given pile length, the shaft capacity increases
413 with an increase in temperature and decreases as the flow rate changes from hydrostatic to
414 infiltration for 5 °C and 25 °C and nonmonotonically varies at 45 °C. For all flow rates, at the
415 reference temperature, the shaft capacity monotonically decreases with a decrease in the pile
416 embedment length due to the reduction in the surface area available for mobilizing shaft capacity.
417 However, at elevated temperatures, the variation of shaft capacity with the pile embedment length
418 is non-monotonic. First, the shaft capacity increases with greater pile embedment length but after
419 reaches a peak value a decrease is observed with further increases in the pile embedment length.
420 This could be due to the domination of changes in effective stress in piles with larger embedment
421 lengths over the decrease in pile surface area available for shaft capacity mobilization. Beyond the
422 peak value, with further increases of the pile embedment depth, the effects of the pile surface area
423 available for side shear mobilization prevails over the effects of the effective stress on shaft
424 capacity.

425 As shown in Fig. 5b, for a given length, the end bearing capacity increases as the
426 temperature increases from 5 to 25 °C and nonmonotonically varies at 45 °C and decreases as the
427 flow rate changes from 0 hydrostatic conditions to positive values (downward infiltration). The
428 effect of temperature on the end bearing capacity increases as the pile embedment length decreases.
429 This could be due to a lower variation of effective stress with the temperature near the water table

430 and a higher variation of effective stress with temperature away from the water table. For all flow
431 rates, at temperatures 5 °C and 25 °C, the end bearing capacity monotonically increases, and at 45
432 °C it increases reaches a peak, and then decreases with a decrease in the pile embedment length,
433 overall, it follows the trend of effective stress.

434 Fig. 5c depicts that the temperature dependency of the ultimate bearing capacity of the pile
435 in clay is controlled by thermal induced changes in the shaft and end bearing capacities. For a
436 given pile embedment length, the ultimate bearing capacity increases with an increase in
437 temperature from 5 °C to 25 °C and 45 °C. For the reference temperature (5 °C), the ultimate
438 bearing capacity decreases monotonically with a decrease in the pile embedment length. At
439 elevated temperatures (25 °C and 45 °C), similar to the trend of shaft capacity, the ultimate bearing
440 capacity non-monotonically varies with the pile embedment length. The percentage of increase in
441 the ultimate bearing capacity by changing temperature increases as the flow rate changes from
442 hydrostatic to infiltration. For example, at a depth of 12 m from the ground surface, the ultimate
443 bearing capacity increases approximately by 13% and 27%, 24% and 53%, and 43% and 95%, by
444 increasing temperature from 5 to 25 and 45 °C under flow rates of zero, -1.6×10^{-9} m/s, and -3.0×10^{-9}
445 m/s, respectively. The increase in the ultimate bearing capacity of pile in clay with an increase in
446 temperature can be attributed to the thermally induced reductions in the degree of saturation, which
447 can increase matric suction in the soil surrounding the pile thus increasing the apparent cohesion,
448 effective stress, and the pile capacities at a given elevated temperature. The changes in effective
449 saturation and matric suction with temperature are due to temperature induced changes in the
450 surface tension, contact angle, and wettability of soil (Grant and Salehzadeh 1996; Vahedifard et
451 al. 2018, 2019).

452 Fig. 6 shows the effective saturation, matric suction, and effective stress of Bonny silt
453 (hereafter referred to as silt) soil with the pile embedment length at temperatures 5, 25, and 45 °C
454 under three flow rates of zero (hydrostatic), -3.2×10^{-8} m/s (infiltration), and -6.0×10^{-8} m/s
455 (infiltration). Similar to the clay, for a given temperature, at different lengths, as we move from
456 the saturated state to unsaturated state, the effective saturation decreases, and matric suction
457 increases. Unlike clay, however, two different trends were observed for effective stress along the
458 pile length with temperature: (a) variation along the pile embedment length at a given temperature
459 and (b) variation with the temperature at a given pile embedment length. First, the effective stress
460 at reference temperature increases monotonically and at elevated temperatures, it increases reaches
461 a peak, and decreases with further reduction in pile embedment length. Second, at depths close to
462 the ground surface, the effective stress decreases, and at depths close to the water table it increases
463 with an increase in temperature. At relatively lower pile embedment lengths, the rate of thermal
464 induced increase in effective stress is higher whereas, at greater embedment lengths, the
465 temperature has a less pronounced effect on effective stress. The trend at elevated temperatures is
466 the same for all flow rates. Compared to clay (Fig. 4), there is a higher reduction in effective
467 saturation with temperature in silt, which could be due to higher permeability and pore size
468 characteristics for silt.

469 Fig. 7 shows the shaft capacity, end bearing capacity, and ultimate bearing capacity of pile
470 in unsaturated silt with pile embedment length at different temperatures and flow rates with $AR =$
471 10. The trends of the shaft, end bearing, and ultimate bearing capacities are different from clay.
472 That is, the variation of shaft, end, and ultimate bearing capacities are monotonic at the reference
473 temperature but become non-monotonic (increase/decrease) under elevated temperatures with the
474 pile embedment length. The behavior of pile capacities is mainly controlled by both effective stress

475 and pile embedment length. The increase is due to drying-induced increase of effective stress and
476 transit to decrease after attaining peak is due to wetting induced reduction of effective stress. A
477 similar type of transition (may be termed as a funicular water regime where the liquid water phase
478 appears to be in a continuous state) occurs in unsaturated soil properties such as soil water retention
479 curve, thermal conductivity function, Poisson's ratio, and others. The range and variation of pile
480 capacities along the pile embedment length are lower compared to clay. This distinct behavior
481 could be due to the range of effective stress and hence apparent cohesion with temperature and
482 pile length. For instance, at a depth of 12 m from the ground surface, the pile ultimate axial
483 capacities vary by approximately 1% and 19%, -5% and -12%, and -29% and -18%, when
484 increasing temperature from 5 to 25 and 45 °C under flow rates of zero, -1.6×10^{-9} m/s, and
485 -3.0×10^{-9} m/s, respectively. For elevated temperatures, the different flow rates have a similar effect
486 on the ultimate bearing capacity.

487 **Effect of Aspect Ratio**

488 For each soil, three different aspect ratios were examined: AR = 5, 10, and 20. To isolate the effect
489 of aspect ratio, the flow rate was kept to $q = 0$ (hydrostatic) in this section. Fig. 8 shows the
490 variation of shaft capacity, end bearing capacity, and ultimate bearing capacity versus the pile
491 embedment length for clay at temperatures 5, 25, and 45 °C and ARs of 5, 10, and 20. Since the
492 suction, effective saturation and effective stress profiles are independent of ARs, they are the same
493 as shown in Fig. 4 for the zero flow rate.

494 For all ARs, the shaft and ultimate bearing capacities of the pile in clay change non-
495 monotonically, and the end bearing capacity of the pile monotonically changes at a given
496 temperature. The temperature dependency of the ultimate bearing capacity is less at the water table
497 (near saturated state) and close to the ground surface. This can be interpreted as the effects of

498 temperature on the pile capacity are the largest in the capillary regime of the SWRC. Further, the
499 impact of temperature on the ultimate bearing capacity increases as AR decreases because of the
500 higher surface area of the pile available for shaft capacity. For higher AR , the temperature has
501 minimal effect on ultimate bearing capacity. For instance, for a 12 m long pile, the ultimate bearing
502 capacity increases approximately by 13% and 27%, 13% and 28%, and 12% and 26%, by
503 increasing temperature from 5 to 25 and 45 °C under AR s of 5, 10, and 20, respectively.

504 Fig. 9 shows the variation of the shaft, end bearing, and ultimate bearing capacities with
505 pile embedment depths for silt at temperatures 5, 25, and 45 °C and AR s of 5, 10, and 20 under no-
506 flow conditions. The suction, effective saturation, and effective stress profiles are the same as
507 shown in Fig. 6 for the zero flow rate case. The shaft, end bearing, and ultimate bearing capacities
508 nonmonotonically vary with temperature along the pile embedment length. For all temperatures,
509 the shaft, end, and ultimate bearing capacities have a similar trend versus the pile embedment
510 length. They first slightly increase close to the water table, reaches a peak, and then decrease.
511 Unlike clay, the percent increase in pile capacities with temperature in silt remains approximately
512 the same for all AR s. For example, at a pile embedment length of 10 m, the pile capacities decrease
513 between 4% to 21% by increasing temperature from 5 °C to 45 °C regardless of AR s. On the other
514 hand, at a specific pile embedment length, the variation of AR s is shown to have a higher impact
515 on pile capacities compared to elevated changes in temperature.

516 Most of the existing studies focused on saturated state and neglected the unsaturated
517 conditions. It is evident from the current study that, for $q = -3.0 \times 10^{-9}$ m/s, at a pile embedment
518 depth of 10 m, the ultimate bearing capacity of pile in unsaturated clay ($S = 90\%$) changes by -
519 27%, 9%, and 63% relative to the saturated conditions ($S = 100\%$) for temperatures 5 °C, 25 °C,
520 and 45 °C, respectively. Similarly, for $q = -6.0 \times 10^{-8}$ m/s, at a pile embedment depth of 10 m, the

521 ultimate bearing capacity of pile in unsaturated silt ($S = 80\%$) varies by -20%, 4%, and 43%
522 relative to saturated conditions ($S = 100\%$) for temperatures 5 °C, 25 °C, and 45 °C, respectively.

523 **CONCLUSIONS**

524 This paper introduced an analytical model to estimate the ultimate bearing capacity of energy piles
525 in unsaturated fine-grained soils under different temperatures and steady flow rates. For this
526 purpose, the formulations for temperature-dependent matric suction and effective saturation were
527 incorporated for calculating shaft capacity, end bearing capacity, and the ultimate bearing capacity
528 of energy piles in unsaturated soils subject to different temperatures. To simplify the model, it was
529 assumed that the soil did not change in volume with heating and that temperature effects on the
530 matric suction and effective saturation were sufficient to capture the effects of thermal induced
531 drying of unsaturated soils. The results of the proposed model were validated against one set of
532 experimental data available in the literature. Further to demonstrate the temperature dependency
533 of the ultimate bearing capacity, a parametric study was conducted with clayey and silty soils at
534 temperatures of 5, 25, and 45 °C and three flow rates (one hydrostatic and two infiltrations) and
535 three aspect ratios (5, 10, and 20). The results were presented in the form of shaft capacity, end
536 bearing capacity, and ultimate bearing capacity along the embedment length of the pile. The results
537 suggested that temperature changes can have a notable effect on matric suction and effective
538 saturation and thereby the ultimate bearing capacity of the pile. For clay, an increase in the
539 effective stress and the ultimate pile bearing capacity is observed under elevated temperatures. For
540 silt, at elevated temperatures, a nonmonotonic behavior of effective stress and hence the ultimate
541 bearing capacity is noted. At a given temperature, for clay, the ultimate bearing capacity decreases,
542 and for silt, it increases/decreases based on the pile embedment length, as the flow rate changes

543 from hydrostatic to infiltration conditions. Further, the bearing capacity increases as the aspect
544 ratio decreases.

545 The study highlighted the considerable impacts of temperature on parameters related to
546 hydraulic conductivity and apparent cohesion of unsaturated soils that could control the ultimate
547 bearing capacity of energy piles under elevated temperatures. The proposed analytical model
548 provides an effective approach to estimate the ultimate bearing capacity of energy piles under
549 various thermal and hydraulic loadings as part of a soil-structure interaction design process. Future
550 studies are suggested to collect more experimental data of ultimate bearing capacity at various
551 effective saturations under drained and undrained thermal, hydraulic, and mechanical loading
552 cases. Such data can be employed to further validate the proposed model.

553 **ACKNOWLEDGMENT**

554 This material is based upon work supported by the National Science Foundation under Grant No.
555 CMMI-1634748. Any opinions, findings, and conclusions or recommendations expressed in this
556 material are those of the authors and do not necessarily reflect the views of the National Science
557 Foundation.

558 **DATA AVAILABILITY STATEMENT**

559 All data, models, and code generated or used during the study appear in the submitted article.

560 **REFERENCES**

561 Akrouch, G. A., Sánchez, M., and Briaud, J. L. (2014). “Thermo-mechanical behavior of energy piles in
562 high plasticity clays.” *Acta Geotechnica*, 9(3), 399-412.

563 Akrouch, G. A., Sánchez, M., and Briaud, J. L. (2016). “An experimental, analytical and numerical study
564 on the thermal efficiency of energy piles in unsaturated soils.” *Computers and*
565 *Geotechnics*, 71(December), 207-220.

566 Başer, T., Dong, Y., Moradi, A. M., Lu, N., Smits, K., Ge, S., D. Tartakovsky, and McCartney, J. S. (2018).
567 Role of nonequilibrium water vapor diffusion in thermal energy storage systems in the vadose
568 zone. *Journal of Geotechnical and Geoenvironmental Engineering*, 144(7), 04018038.

569 Behbehani, F. and McCartney, J.S. (2020a). “Impacts of unsaturated conditions on the ultimate axial
570 capacity of energy piles.” *EUnsat 2020: The 4th European Conference on Unsaturated Soils*.
571 Lisbon, Portugal. Jun. 24-26. E3S Web Conf., Paris. Vol. 195, 04005. pp. 1-6. DOI:
572 <https://doi.org/10.1051/e3sconf/202019504005>.

573 Behbehani, F. and McCartney, J.S. (2020b). “Simulation of the thermo-hydraulic response of energy piles
574 in unsaturated soils.” *Proc. 2nd International Conference on Energy Geotechnics (ICEGT-2020)*.
575 La Jolla, CA. Mar. 28-31, 2021. E3S Web of Conferences, Les Ulis, France. pp. 1-6.

576 Bishop, A. W. (1959). “The principle of effective stress”. *Teknisk Ukeblad*, 39, 859-863.

577 Bourne-Webb, P. J., Amatya, B., Soga, K., Amis, T., Davidson, C., and Payne, P. (2009). “Energy pile test
578 at Lambeth College, London: Geotechnical and thermodynamic aspects of pile response to heat
579 cycles.” *Géotechnique*, 59(3), 237–248.

580 Brandl, H. (2006). “Energy foundations and other thermo-active ground structures.” *Géotechnique*, 56(2),
581 81–122.

582 Brooks, R. H., and A. T. Corey. (1964). *Hydraulic properties of porous media: Hydrology paper No. 3*.
583 Fort Collins, CO: Colorado State Univ.

584 Burland J. B. (1973). “Shaft friction of piles in clay-a simple fundamental approach.” *Ground Engineering*,
585 6-3, 30-42.

586 Campbell, G. S., Jungbauer Jr, J. D., Bidlake, W. R., and Hungerford, R. D. (1994). Predicting the effect
587 of temperature on soil thermal conductivity. *Soil Science*, 158(5), 307-313.

588 Chandler R. J. (1968). "The shaft friction of piles in cohesive soils in terms of effective stress," *Civil*
589 *Engineering and Public Works Review*. 63, 48-51.

590 Chen, D. and McCartney, J. S. (2017). "Parameters for load transfer analysis of energy piles in uniform
591 nonplastic soils." *ASCE International Journal of Geomechanics*. 17(7), 04016159. DOI:
592 10.1061/(ASCE)GM.1943-5622.0000873.

593 Constantz, J. (1982). "Temperature Dependence of Unsaturated Hydraulic Conductivity of Two Soils
594 1." *Soil Science Society of America Journal*, 46(3), 466-470.

595 Di Donna, A., and Laloui, L. (2013). "Soil response under thermomechanical conditions imposed by energy
596 geostructures." *Energy Geotechniques: Innovation in Underground Engineering*, 3-21.

597 Di Donna, A., Ferrari, A., and Laloui, L. (2016b). "Experimental investigations of the soil–concrete
598 interface: physical mechanisms, cyclic mobilization, and behaviour at different temperatures."
599 *Canadian Geotechnical Journal*, 53: P659-672.

600 Di Donna, A., Loria, A. F. R., and Laloui, L. (2016a). "Numerical study of the response of a group of
601 energy piles under different combinations of thermo-mechanical loads." *Computers and*
602 *Geotechnics*, 72, 126-142.

603 Dorsey, N. E. (1940). *Properties of Ordinary Water Substance*. New York: Reinhold.

604 Elzeiny, R., Suleiman, M. T., Xiao, S., Abu Qamar, M. A., & Al-Khawaja, M. (2020). "Laboratory-scale
605 pull-out tests on a geothermal energy pile in dry sand subjected to heating cycles." *Canadian*
606 *Geotechnical Journal*. <https://doi.org/10.1139/cgj-2019-0143>.

607 Fu, Z. (2017). *Thermo-Hydro-Mechanical Effects on the Behaviour of Unsaturated Soil-Structure*
608 *Interfaces and the Numerical Analysis of Energy Piles*. Doctoral dissertation, Université
609 d'Ottawa/University of Ottawa.

610 Fuentes, R., Pinyol, N., and Alonso, E. (2016). "Effect of temperature induced excess porewater pressures
611 on the shaft bearing capacity of geothermal piles." *Geomechanics for Energy and the*
612 *Environment*, 8, 30-37.

613 Gardner, W. R. (1958). "Steady state solutions of the unsaturated moisture flow equation with application
614 to evaporation from a water table," *Soil Sci.*, 85, 228–232.

615 Georgiadis, K., Potts, D. M., and Zdravkovic, L. (2003). "The influence of partial soil saturation on pile
616 behaviour." *Géotechnique*, 53(1), 11-25.

617 Goode III, J. C., and McCartney, J. S. (2015). "Centrifuge modeling of end-restraint effects in energy
618 foundations." *Journal of Geotechnical and Geoenvironmental Engineering*, 141(8), 04015034.

619 Graham, J., Tanaka, N., Crilly, T., and Alfaro, M. (2001). "Modified Cam-Clay modelling of temperature
620 effects in clays." *Canadian Geotechnical Journal*, 38(3), 608-621.

621 Grant, S. A. (2003). Extension of a temperature effects model for capillary pressure saturation
622 relations. *Water Resources Research*, 39(1), SBH 1-10.

623 Grant, S. A., and Salehzadeh, A. (1996). "Calculation of temperature effects on wetting coefficients of
624 porous solids and their capillary pressure functions." *Water Resources Research*, 32(2), 261-270.

625 Haar, L., Gallagher, J. S. and Kell, G. S. (1984). *NBS/NRC steam table*. New York: Hemisphere Publishing
626 Corporation.

627 Hueckel, T., Pellegrini, R., and Del Olmo, C. (1998). A constitutive study of thermo- elasto- plasticity of
628 deep carbonatic clays. *International journal for numerical and analytical methods in*
629 *geomechanics*, 22(7), 549-574.

630 Kalantidou, A., Tang, A. M., Pereira, J. and Hassen, G. (2012). "Preliminary study on the mechanical
631 behaviour of heat exchanger pile in physical model." *Géotechnique*, 62(11), 1047–1051

632 Knellwolf, C., Peron, H., and Laloui, L. 2011. "Geotechnical analysis of heat exchanger piles." *Journal of*
633 *Geotechnical and Geoenvironmental Engineering*, 137 (10): P890–902

634 Kramer, C. A., and Basu, P. (2014). Performance of a model geothermal pile in sand. In *Proc. 8th Int. Conf.*
635 *on Physical Modelling in Geotechnics*, Perth (Gaudin, C. & White, D.(eds)). Leiden: CRC
636 Press/Balkema (pp. 771-777).

637 Laloui, L., and Loria, A. F. R. (2019). *Analysis and Design of Energy Geostructures: Theoretical Essentials*
638 *and Practical Application*. Academic Press.

639 Laloui, L., Nuth, M., and Vulliet, L. (2006). Experimental and numerical investigations of the behaviour of
640 a heat exchanger pile. *International Journal for Numerical and Analytical Methods in*
641 *Geomechanics*, 30(8), 763-781.

642 Li, C., Kong, G., Liu, H., and Abuel-Naga, H. (2019). “Effect of temperature on behaviour of red clay–
643 structure interface.” *Canadian Geotechnical Journal*, 56(1), 126-134.

644 Lide, D. R. (1995). *Handbook of Chemistry and Physics*, 75th edn. CRC Press, New York.

645 Liu, H. L., Wang, C. L., Kong, G. Q., and Bouazza, A. (2019). “Ultimate bearing capacity of energy piles
646 in dry and saturated sand.” *Acta Geotechnica*, 14(3), 869-879.

647 Loveridge, F. A., Narsilio, G., Sánchez, M., and McCartney, J. S. (2019). “Energy geostructures: a review
648 of analysis approaches, in situ testing and model scale experiments.” *Geomechanics for Energy*
649 *and the Environment*. 22, 100173, 1-30.

650 Lu, N., and Griffiths, D. V. (2004). Profiles of steady-state suction stress in unsaturated soils. *Journal of*
651 *Geotechnical and Geoenvironmental Engineering*, 130(10), 1063-1076.

652 Lu, N., Godt, J. W., and Wu, D. T. (2010). “A closed- form equation for effective stress in unsaturated
653 soil.” *Water Resources Research*, 46(5).

654 McCartney, J. S. and Murphy, K. D. (2017). Investigation of potential dragdown/uplift effects on energy
655 piles. *Geomechanics for Energy and the Environment*. 10(June), 21-28.

656 McCartney, J. S., and Rosenberg, J.E. (2011). Impact of heat exchange on side shear in thermo-active
657 foundations. In *Geo-Frontiers 2011: Advances in Geotechnical Engineering*. 488-498.

658 McCartney, J. S., Jafari, N. H., Hueckel, T., Sanchez, M., and Vahedifard, F. (2019). Thermal energy issues
659 in geotechnical engineering. *Geotechnical Fundamentals for Addressing New World Challenges*.
660 N. Lu and J.K. Mitchell, Eds. Springer. 275-317.

661 Murphy, K.D. and McCartney, J.S. (2014). “Thermal borehole shear device.” *ASTM Geotechnical Testing*
662 *Journal*. 37(6), 1040-1055.

663 Murphy, K.D., McCartney, J.S., and Henry, K.S. (2015). “Evaluation of thermo-mechanical and thermal
664 behavior of full-scale energy foundations.” *Acta Geotechnica*. 10(2), 179 195.

665 Ng, C. W. W., Shi, C., Gunawan, A., Laloui, L., and Liu, H. L. (2015). "Centrifuge modelling of heating
666 effects on energy pile performance in saturated sand." *Canadian Geotechnical Journal*, 52(8),
667 1045-1057.

668 Olgun, C.G., Ozudogru, T.Y., Abdelaziz, S. L., and Senol, A. (2014). "Long-term performance of heat
669 exchanger piles." *Acta Geotechnica*. (10), 553–569.

670 Ozudogru, T. Y., Olgun, C. G., & Arson, C. F. (2015). "Analysis of friction induced thermo-mechanical
671 stresses on a heat exchanger pile in isothermal soil." *Geotechnical and Geological*
672 *Engineering*, 33(2), 357-371.

673 Philip, J. R. (1969). Theory of infiltration. In *Advances in Hydroscience*, Elsevier, 5, 215-296.

674 Philip, J. R., and De Vries, D. A. (1957). Moisture movement in porous materials under temperature
675 gradients. *Eos, Transactions American Geophysical Union*, 38(2), 222-232.

676 Pillsbury, A. F. (1950). "Effects of particle size and temperature on the permeability of sand to water." *Soil*
677 *Sci.*, 70(4), 299-300.

678 Ravera, E., Sutman, M., and Laloui, L. (2020). "Load transfer method for energy piles in a group with pile–
679 soil–slab–pile interaction." *Journal of Geotechnical and Geoenvironmental Engineering*, 146(6),
680 04020042.

681 Rotta, Loria A.F., Gunawan, A., Shi, C., Laloui, L., and Ng, C.W.W. (2015). "Numerical modelling of
682 energy piles in saturated sand subjected to thermo-mechanical loads." *Geomechanics for Energy*
683 *and the Environment*. 1, 1–15.

684 Saggiu, R., and Chakraborty, T. (2015). "Cyclic thermo-mechanical analysis of energy piles in sand."
685 *Geotech Geol Eng (2015)* 33, 321–342.

686 Skempton A. W. (1959). "Cast-in-situ bored piles in London clay," *Géotechnique*, 9, 153-173.

687 Suryatriyastuti, M. E., Mroueh, H., and Burlon, S. (2013). "Numerical analysis of the bearing capacity of
688 thermoactive piles under cyclic axial loading." Chapter 7, *Energy Geotechniques*, L. Laloui and A.
689 Di Donna, eds., Wiley, London.

690 Suryatriyastuti, M. E., Mroueh, H., and Burlon, S. (2014). "A load transfer approach for studying the cyclic
691 behavior of thermo-active piles." *Computers and Geotechnics*, 55, 378-391.

692 Thota, S. K., Cao, T. D., Vahedifard, F., and Ghazanfari, E. (2019). "Stability analysis of an unsaturated
693 silty slope under nonisothermal conditions." In *Geo-Congress 2019: Geotechnical Materials,
694 Modeling, and Testing*, Reston, VA: American Society of Civil Engineers, 844-852.

695 Thota, S. K., and Vahedifard, F. (2020). "A model for ultimate bearing capacity of piles in unsaturated soils
696 under elevated temperatures." In *E3S Web of Conferences* (Vol. 205, p. 05003). EDP Sciences.

697 Uchaipichat, A. (2005). *Experimental Investigation and Constitutive Modelling of Thermo-hydro-
698 mechanical Coupling in Unsaturated Soils*. PhD Thesis. University of New South Wales, Australia.

699 Uchaipichat, A. (2012). "Variation of pile capacity in unsaturated clay layer with suction." *Electronic
700 Journal of Geotechnical Engineering*, 17, 2425-2433.

701 Uchaipichat, A. (2013). "Pile capacity in silt layer under elevated temperature." *Electronic Journal of
702 Geotechnical Engineering*, 18, 5499-5505.

703 Vahedifard, F., Cao, T. D., Ghazanfari, E., and Thota, S. K. (2019). "Closed-form models for nonisothermal
704 effective stress of unsaturated soils." *Journal of Geotechnical and Geoenvironmental
705 Engineering*, 145(9), 04019053.

706 Vahedifard, F., Cao, T. D., Thota, S. K., and Ghazanfari, E. (2018). "Nonisothermal models for soil–water
707 retention curve." *Journal of Geotechnical and Geoenvironmental Engineering*, 144(9), 04018061.

708 Vahedifard, F., Leshchinsky, D., Mortezaei, K., and Lu, N. (2016). "Effective stress-based limit equilibrium
709 analysis for homogeneous unsaturated slopes." *Int. J. Geomech.*, 10.1061/(ASCE)GM.1943-
710 5622.0000554, D4016003.

711 Vahedifard, F., Thota, S. K., Cao, T. D., Samarakoon, R. A., and McCartney, J. S. (2020). "A temperature-
712 dependent model for small-strain shear modulus of unsaturated soils." *Journal of Geotechnical and
713 Geoenvironmental Engineering*, 146(12): 04020136, DOI: 10.1061/(ASCE)GT.1943-
714 5606.0002406.

715 Vanapalli, S. K., and Taylan, Z. N. (2012). "Design of single piles using the mechanics of unsaturated
716 soils." *International Journal of GEOMATE*, 2(1), 197-204.

717 Vasilescu, A. R., Fauchille, A. L., Dano, C., Kotronis, P., Manirakiza, R., and Gotteland, P. (2019). "Impact
718 of temperature cycles at soil–concrete interface for energy piles." *In International Symposium on*
719 *Energy Geotechnics* (pp. 35-42). Springer, Cham.

720 Wang, B., Bouazza, A., Barry-Macaulay, D., Singh, M. R., Webster, M., Haberfield, C., and Baycan, S.
721 (2012). "Field and laboratory investigation of a heat exchanger pile." *In GeoCongress 2012: State*
722 *of the Art and Practice in Geotechnical Engineering*, pp. 4396-4405.

723 Wang, W., Regueiro, R. A., and McCartney, J. S. (2014). "Coupled axisymmetric thermo-poro-mechanical
724 finite element analysis of energy foundation centrifuge experiments in partially saturated
725 silt." *Geotechnical and Geological Engineering*, 33(2), 373-388.

726 Watson, K. M. (1943). "Thermodynamics of the liquid state." *Ind. Eng. Chem.* 35 (4): 398–406.

727 Xiao, S., Suleiman, M. T., and McCartney, J. S. (2014). "Shear behavior of silty soil and soil-structure
728 interface under temperature effects." *In Geo-Congress 2014: Geo-characterization and Modeling*
729 *for Sustainability* (pp. 4105-4114).

730 Yavari, N., Tang, A. M., Pereira, J. M., and Hassen, G. (2016). "Effect of temperature on the shear strength
731 of soils and the soil–structure interface." *Canadian Geotechnical Journal*, 53(7), 1186-1194.

732 Yazdani, S., Helwany, S., and Olgun, G. (2019). "Influence of temperature on soil–pile interface shear
733 strength." *Geomechanics for Energy and the Environment*, 18, 69-78.

734
735
736
737
738
739
740

741 **List of Figures**

742 **Fig. 1.** Temperature-dependent soil water retention curves for: (a) Bonny silt and (b) Denver
743 bentonite.

744
745 **Fig. 2.** Comparison between predicted versus measured volumetric water content in unsaturated
746 Bonny silt with the measured change in temperature from ambient condition to elevated
747 temperature (measured values reported by Behbehani and McCartney 2020a).

748
749 **Fig. 3.** Energy pile capacities with temperature: (a) predicted shaft capacity, (b) predicted end
750 bearing capacity, and (c) measured and predicted ultimate bearing capacity (measured
751 values from Behbehani and McCartney 2020a).

752
753 **Fig. 4.** Profiles along the pile embedment length in Denver bentonite at three temperatures and
754 three flow rates: (a) effective saturation, (b) matric suction, and (c) effective stress.

755 **Fig. 5.** Profiles versus embedment depth of pile in Denver bentonite at three temperatures and
756 three flow rates: (a) shaft bearing capacity, (b) end bearing capacity, and (c) ultimate
757 bearing capacity.

758 **Fig. 6.** Profiles along the pile embedment depth at the edge of the pile in Bonny silt at three
759 temperatures and three flow rates: (a) effective saturation, (b) matric suction, and (c)
760 effective stress.

761 **Fig. 7.** Profiles versus embedment depth of pile in Bonny silt at three temperatures and three
762 flow rates: (a) shaft bearing capacity, (b) end bearing capacity, and (c) ultimate bearing
763 capacity.

764 **Fig. 8.** Profiles versus embedment depth of pile in Denver bentonite at three temperatures and
765 three aspect ratios: (a) shaft bearing capacity, (b) end bearing capacity, and (c) ultimate
766 bearing capacity.

767 **Fig. 9.** Profiles versus embedment depth of pile in Bonny silt at three temperatures and three
768 aspect ratios: (a) shaft bearing capacity, (b) end bearing capacity, and (c) ultimate bearing
769 capacity.

770

771

772

773

774

775

776

777

778

Table 1. Soil parameters used in the proposed formulation

Saturated			Unsaturated		
Property	Parameter(s)	Relevant tests	Property	Parameter(s)	Relevant tests
Shear strength parameters	$c'_{a,T}, \beta_c$	Conventional shear strength tests	Soil water retention curve parameters	n_{BC}, ψ_{aev}	Water retention tests
Intrinsic permeability	k_{in}	Permeability tests	Enthalpy of immersion	Δh_{T_r}	Calorimetric test

779

780

781

782

783

784

785

786

787

788

789

790

791

792

793

794

795

796

797

798

Table 2. Input parameters for validation and parametric study

Soil	n_{BC}	ψ_{aev} (kPa)	Δh_{r_r} (J/m ²)	β_c	k_{in} (m ²)	$c'_{a,T}$ (kPa)
Bonny silt	0.37	19	-0.45	0.26	1×10^{-14}	0.0
Denver bentonite	0.27	100		0.25	1×10^{-16}	10.0

799

Figure 1

[Click here to access/download;Figure;1.PDF](#) 

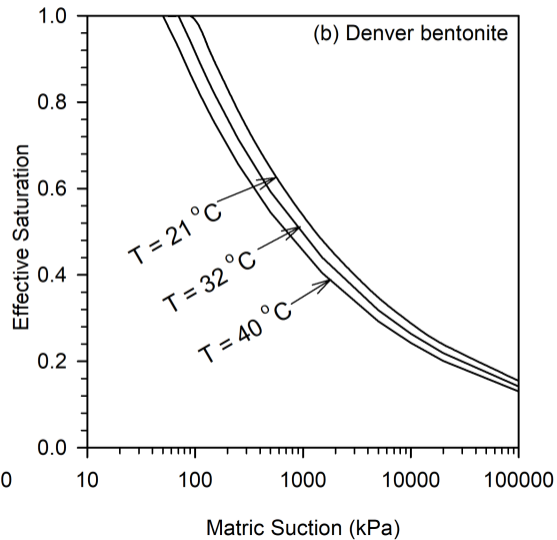
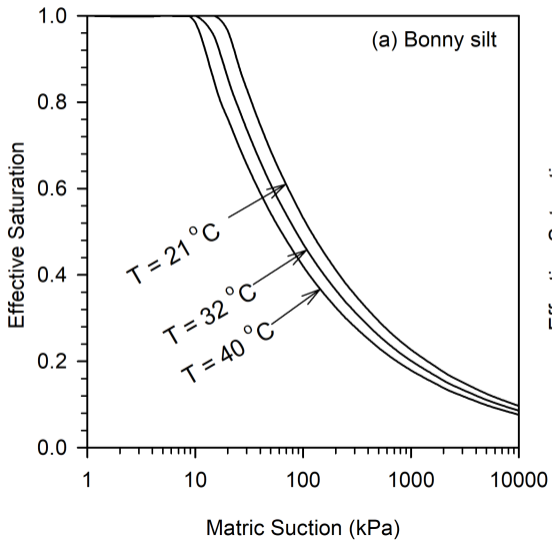


Figure 2

[Click here to access/download;Figure;2.PDF](#)

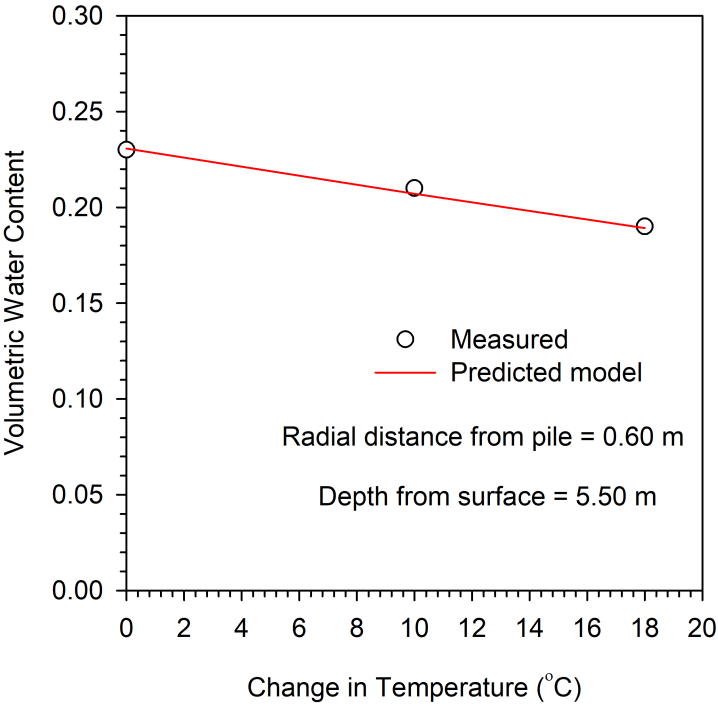


Figure 3

[Click here to access/download;Figure;3.PDF](#)

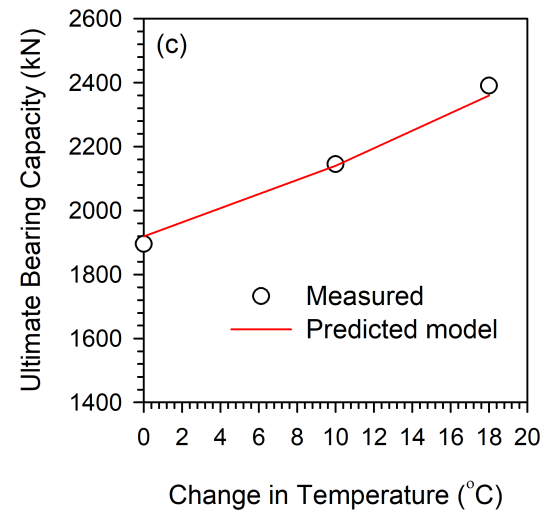
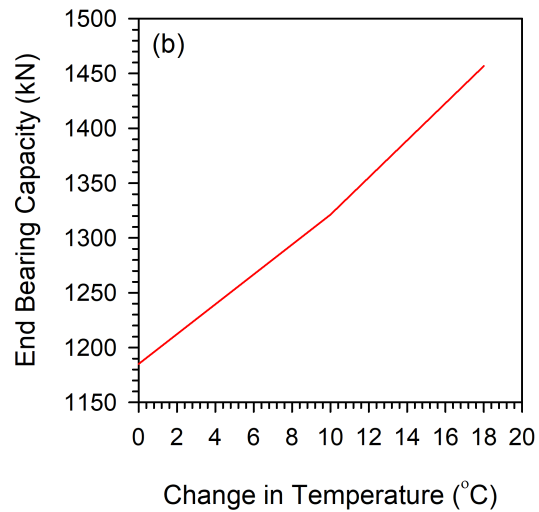
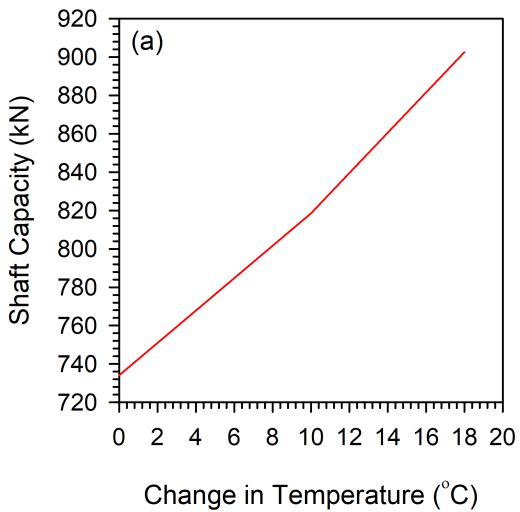


Figure 4 Effective Saturation Matric Suction (kPa) Effective Stress (kPa) [Click here to access/download;Figure;4.PDF](#) 

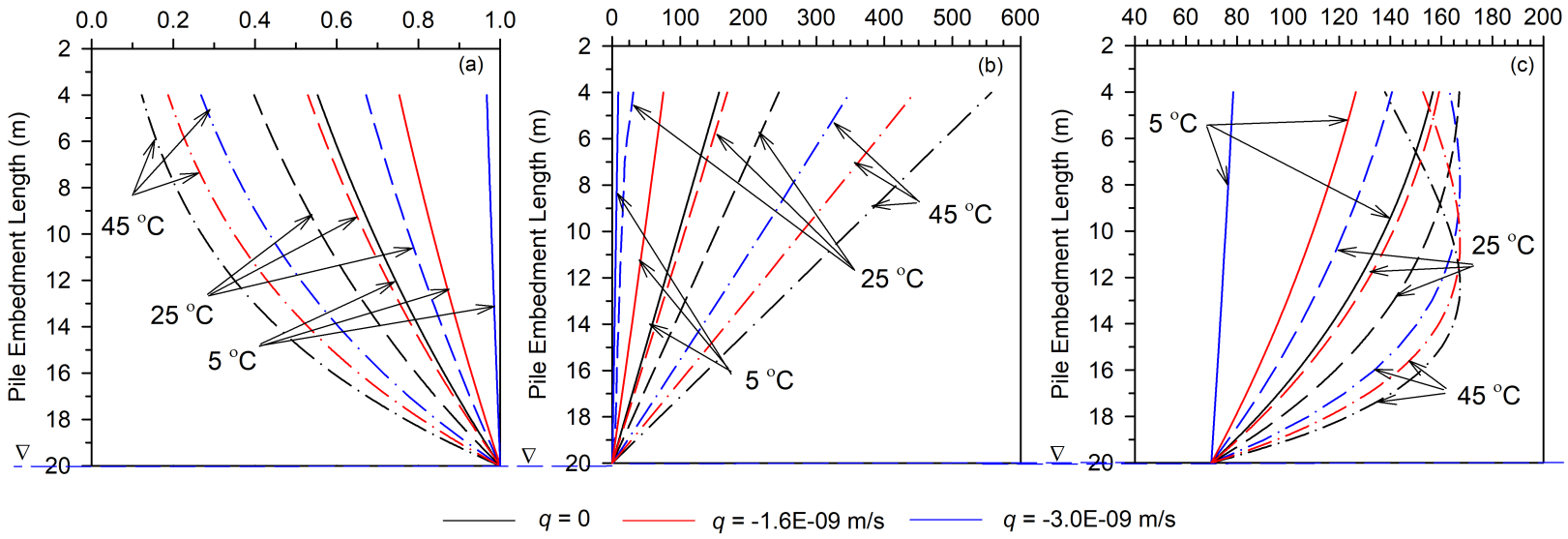
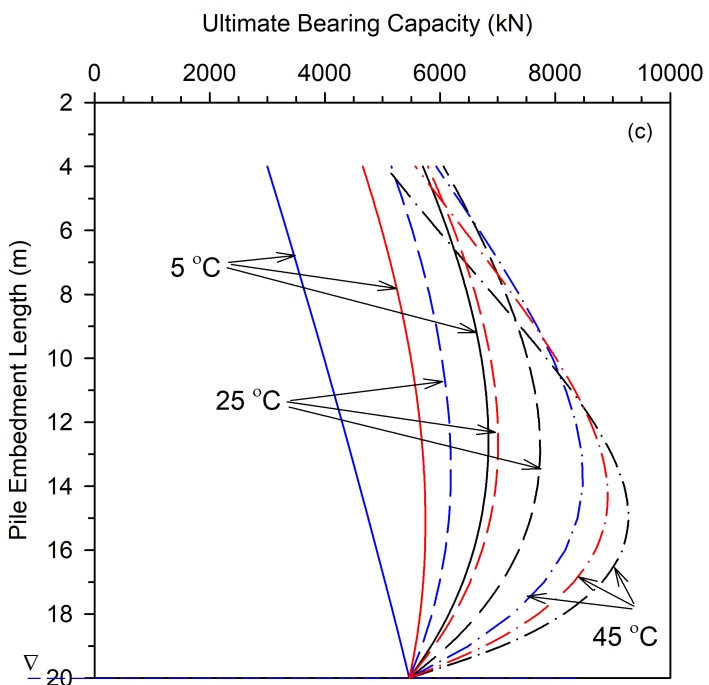
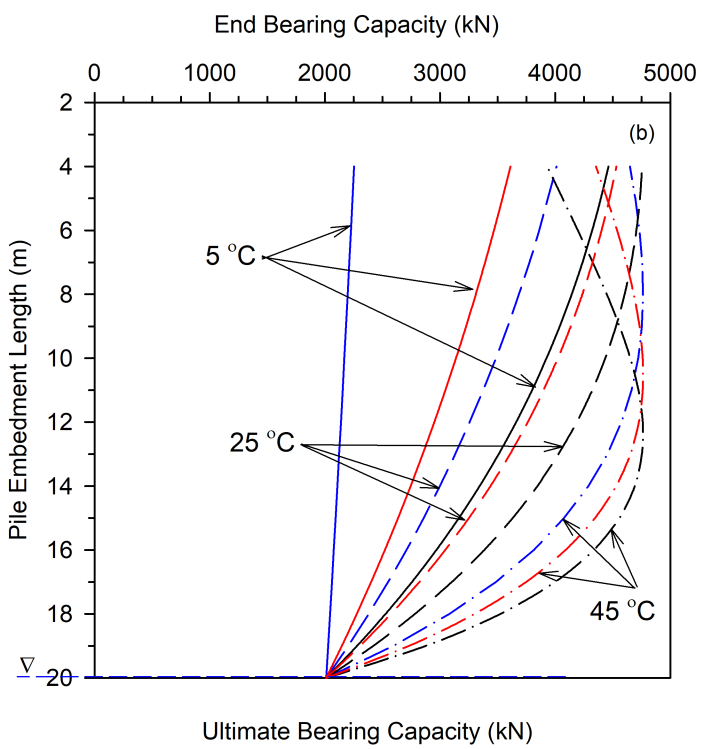
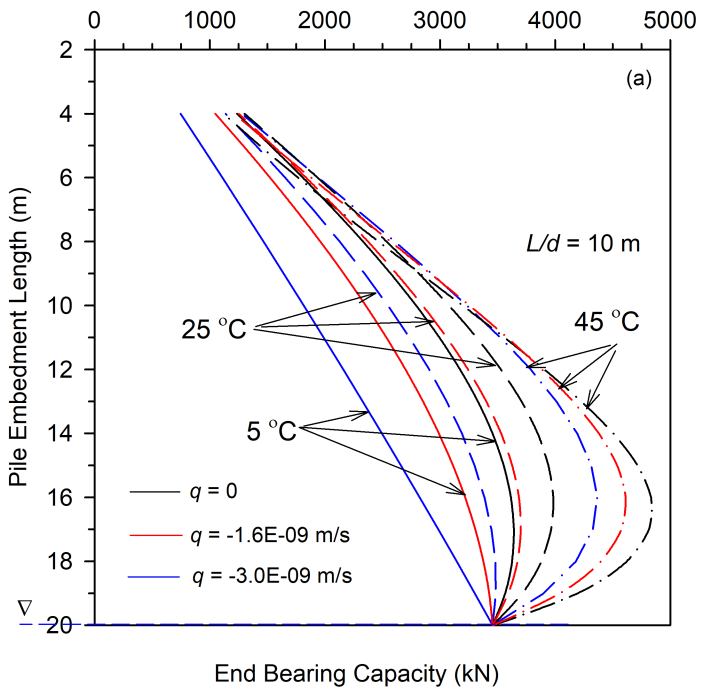


Figure 5



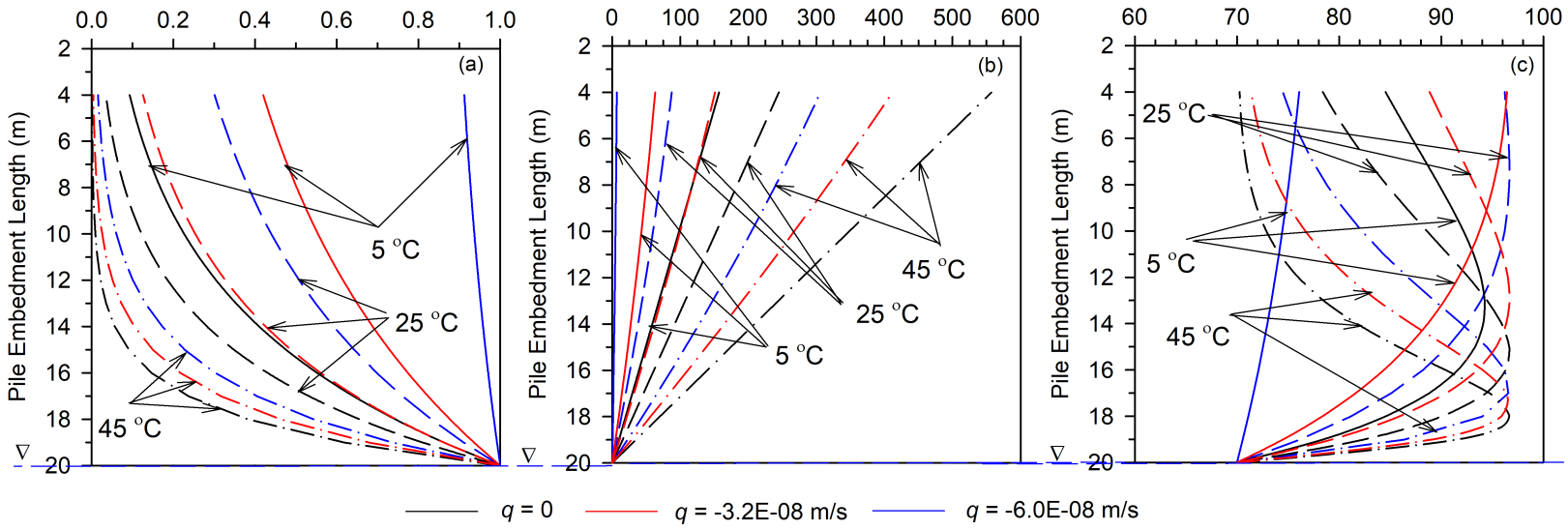


Figure 7

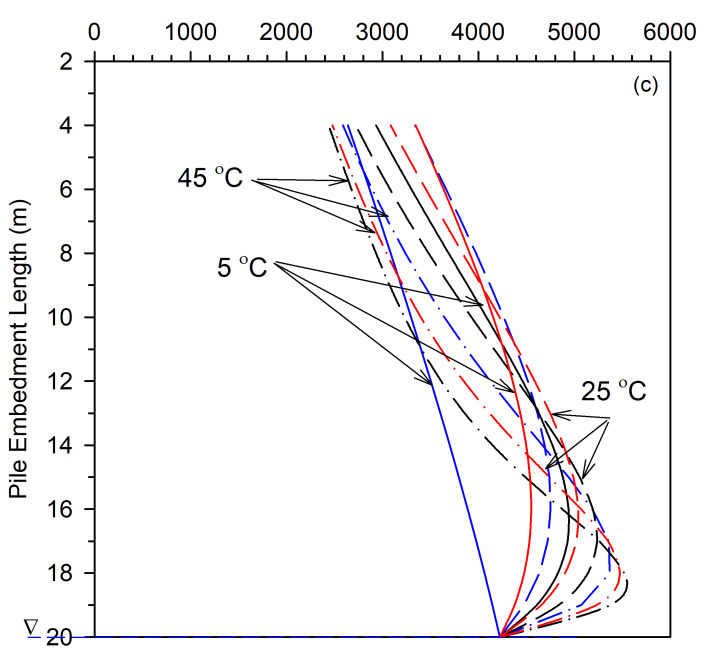
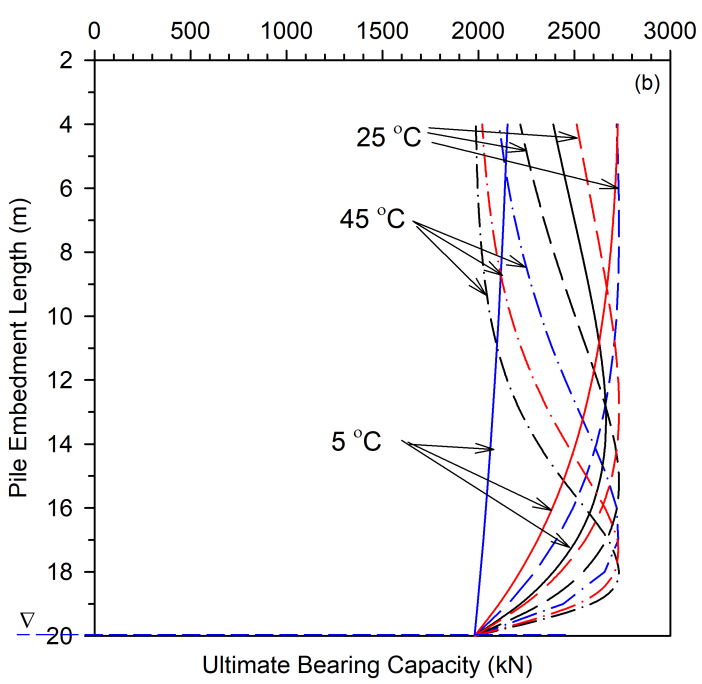
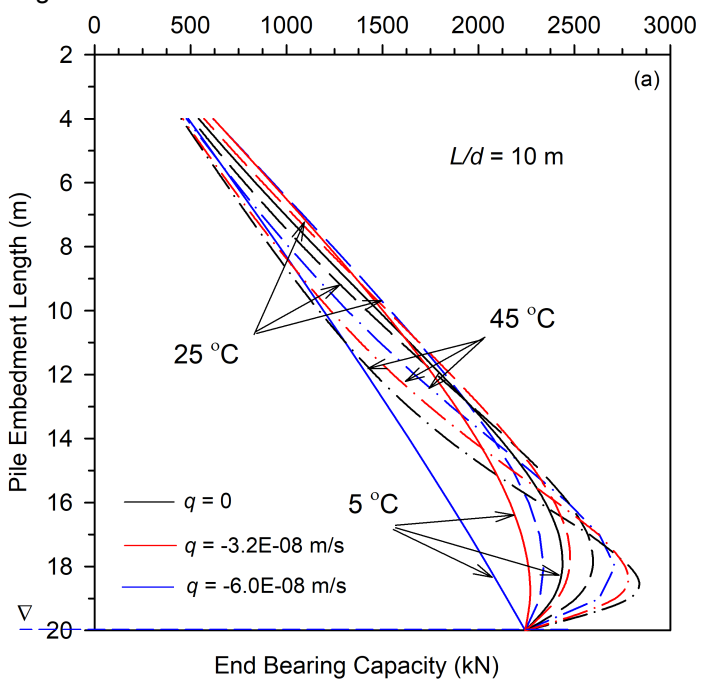


Figure 8

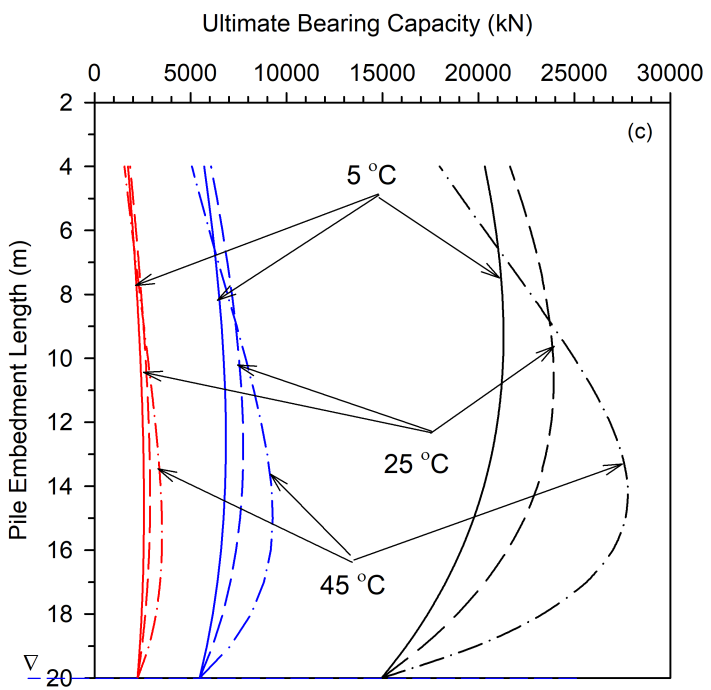
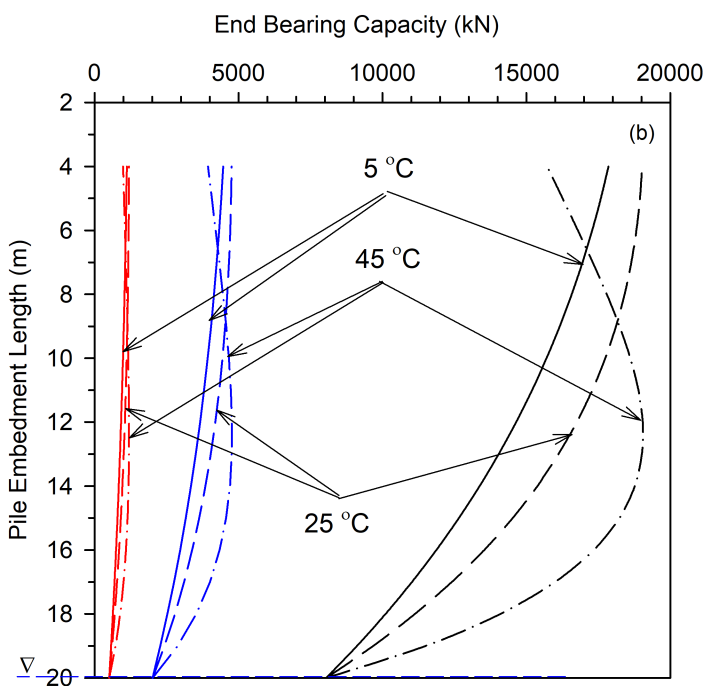
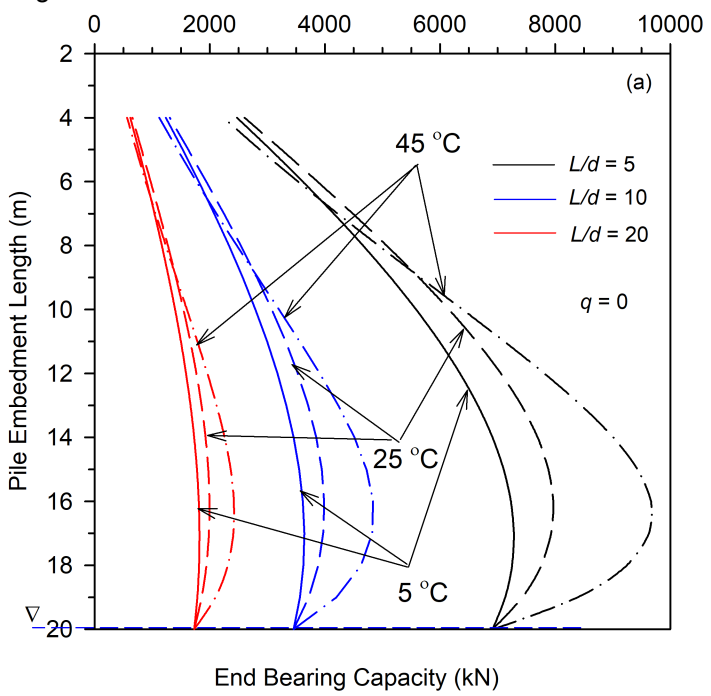


Figure 9

